Latent-heating impact on tides in Middle and Upper Atmosphere Model MUAM

University of Leipzig
Written elaboration
Module Dynamics of the Middle Atmosphere
Winter semester 2020/21

submitted by:

Richard Engelhardt
Matriculation number: 3701280
04.03.2021

Contents

1 Motivation and state of knowledge

Atmospheric tides in the middle and upper atmosphere have larger amplitudes compared to tides at lower elevation levels. The reason for this is conservation of energy due to decreasing density with height. Therefore atmospheric tides in the middle and upper atmosphere are important for atmospheric circulation [Gurubaran, n.d.]. Diurnal tides (DT) are mainly excited by absorption of water vapor in the troposphere. Semidiurnal tides (SDT) are mainly excited by absoprtion of ozon in the stratosphere [Andrews *et al.*, 1987]. Both DT and SDT have larger amplitudes than higher order tides, for example terdiurnal tides (TDT) and quarterdiurnal tides (QDT).
Latent heat is not evenly distributed on earth. It forces non-migrating tidal modes which propagate into the upper atmosphere [Williams & Avery, 1996]. The magnitude of these non-migrating components can evolve from month to month [Hagan & Forbes, 2002]. Among other things, latent heat acts as a forcing mechanism for TDT and QDT [Forbes *et al.*, 1997; Zhang *et al.*, 2006]. Variations of tides due to latent heat are most apparent at 80 km to 150 km height. Amplitude variations of wind velocitiy and temperature can reach 10 $\mathrm{m\,s^{-1}}$ to 20 $\mathrm{m\,s^{-1}}$ and 5 K to 15 K for DT and SDT [Hagan & Forbes, 2002, 2003]. According to Williams & Avery [1996] solar heating and latent heat release contributions are comparable in production of atmospheric tides at certain locations. The findings to date show that variation of latent heat has a significant effect on atmospheric tides [Hamilton, 1981; Williams & Avery, 1996; Forbes *et al.*, 1997; Hagan & Forbes, 2002].

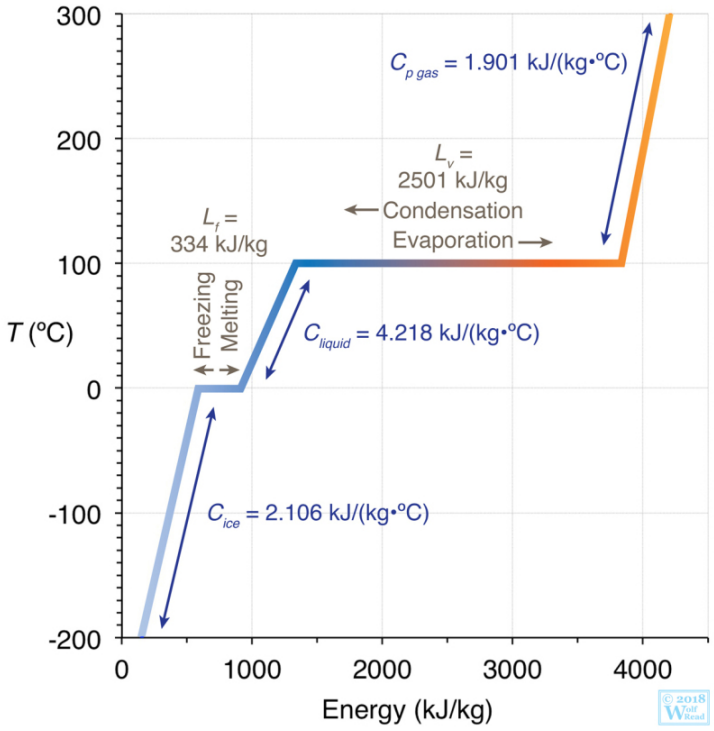

Figure 1: Temperature in °C depending on the required energy in $\mathrm{kJ\,kg^{-1}}$ for phase transitions of water from Stull *et al.* [2018]

2 Basics

2.1 Latent heat

Latent heat is the heat of transformation consumed or released during the change of aggregate states. Since it is an issue of the atmosphere, aggregate states of water are considered. There are heat of evaporation/condensation, melting/freezing and deposition/sublimation.

Figure 1 shows the amount of required energy for heating ice to liquid water and heating liquid water to water vapor. Beginning from ice the temperature increases with increasing energy. The energy is consumed for the temperature rise of the ice. At the certain threshold of 0 °C the temperature remains constant with increasing energy. The amount of energy without a change of temperature is the heat of transformation by melting/freezing. As soon as the change of aggregate state is finished, the temperature again increases with increasing energy. Now the energy is consumed for the temperature rise of the liquid water. At the next threshold of 100 °C the temperature once more remains constant with increasing energy. The amount of energy without a change of temperature is the heat of transformation by evaporation/condensation. After a certain amount of energy, needed for change of aggregate state, the temperature increases with increasing energy. The energy is consumed for the temperature rise of the water vapor. The temperature threshold values depend on the surrounding pressure.

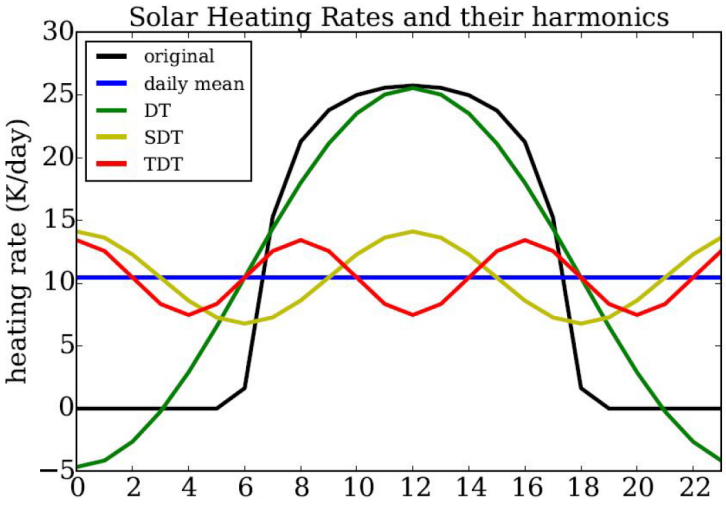

Figure 2: Solar heating rate of the sun (black) in K day^{-1} depending on the time of the day for 2.5° north latitude and 50 km height, Fourier analysis of black curve shows harmonic oscillations with periods of 24 hours (green), 12 hours (yellow) and 8 hours (red), the blue line represents the daily average, from Lilienthal [2019]

The amount of energy is 2501 kJ kg^{-1} for evaporation/condensation and 334 kJ kg^{-1} for melting/freezing. The prevailing source of humidity in the tropical and subtropical troposphere is convective precipitation in clouds under deep convection [Ermakova *et al.*, 2019]. Thus the main source of latent heat is evaporation and condensation.

2.2 Atmospheric tides

Atmospheric tides are an important large-scale mechanism for transporting energy from the lower atmosphere into the upper. The kinetic energy must be conserved while propagating into the upper atmosphere. Due to density decrease with height, the amplitude increases. Atmospheric tides are excited by solar heating, gravity by moon or sun, nonlinear interactions between tides or planetary waves and latent heat [Andrews *et al.*, 1987; Forbes *et al.*, 1995]. The impact of gravity of the sun or moon on atmospheric tides is negligible.

Atmospheric tides forced by solar heating are called solar atmospheric tides. The following types are distinguished. There are migrating and non-migrating tides. Migrating tides propagate sun-synchronous, westward with the apparent motion of the sun. Non-migrating tides do not propagate sun-synchronous. Either they do not propagate horizontally, or they propagate eastwards, or they propagate westwards at a different speed to the sun. Non-migrating tides are generated by differences in topography, land-sea contrast or surface interactions [Forbes *et al.*, 2006; Tsuda & Kato, 1989]. However, non-migrating tides are not considered in Middle and Upper Atmosphere Model (MUAM).

Figure 2 shows solar heating rates depending on the time of the day with the minimum solar zenith angle at 12 pm. The black curve shows the heating of the sun with its maxi-

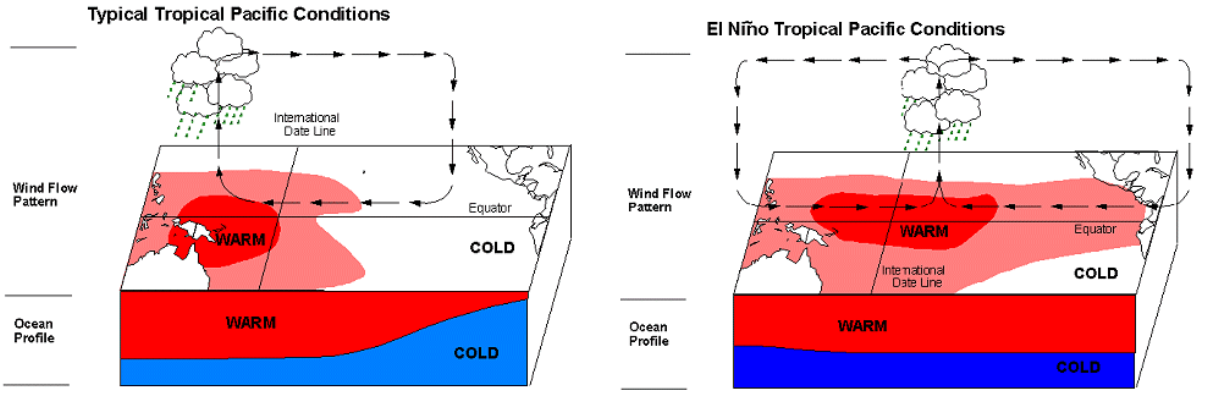

(a) (b)

Figure 3: El Niño-Southern Oscillation, typical tropical Pacific conditions (a), El Niño tropical Pacific conditions (b), from Ammann [2021]

mum value at 12 pm and no heating at night. A Fourier analysis of the black curve shows harmonic oscillations with different periods. The green curve is the DT and has a period of 24 hours. The yellow curve is the SDT and has a period of 12 hours. The red curve is the TDT and has a period of 8 hours. QDT are not shown in this picture, but would have a smaller period of 6 hours and even smaller amplitudes than TDT. Using figure 2 a decreasing amplitude with decreasing period can be identified.

2.3 El Niño-Southern Oscillation

El Niño-Southern Oscillation (ENSO) is a self-reinforcing warm and cold phase by anomalies of the Walker circulation. The phase changes approximately every four years. It is one of strongest natural climate fluctuations with global impacts [Latif, 2006]. El Niño is related to the heating of large parts of the pacific ocean. The Southern Oscillation is connected to the pressure tendencies between the southeast Asian low pressure system and the southeast Pacific high pressure system. It is influenced by the temperature contrast along the tropical pacific ocean and thus by El Niño.
During typical tropical pacific conditions warm water is located northeast of Australia. Above the warm water is a low pressure system. During El Niño tropical pacific conditions the center of the warm water is displaced to the east. There is more warm water in the east on the surface of the pacific ocean compared to typical conditions. The low pressure system is equally relocated to the east. The higher pressure is now located over the west pacific. This leads to a weakening of the Walker circulation and the passat winds. Less cold water rises off the coast of South America. As a consequence there is a further increase of the sea surface temperature. That is the reason why ENSO is self-reinforcing. Precipitation varies spatial with different phase of ENSO. Wind, pressure gradients, and air and water temperature are also impacted by ENSO. There are global impacts due to atmospheric teleconnections, like for example planetary waves.

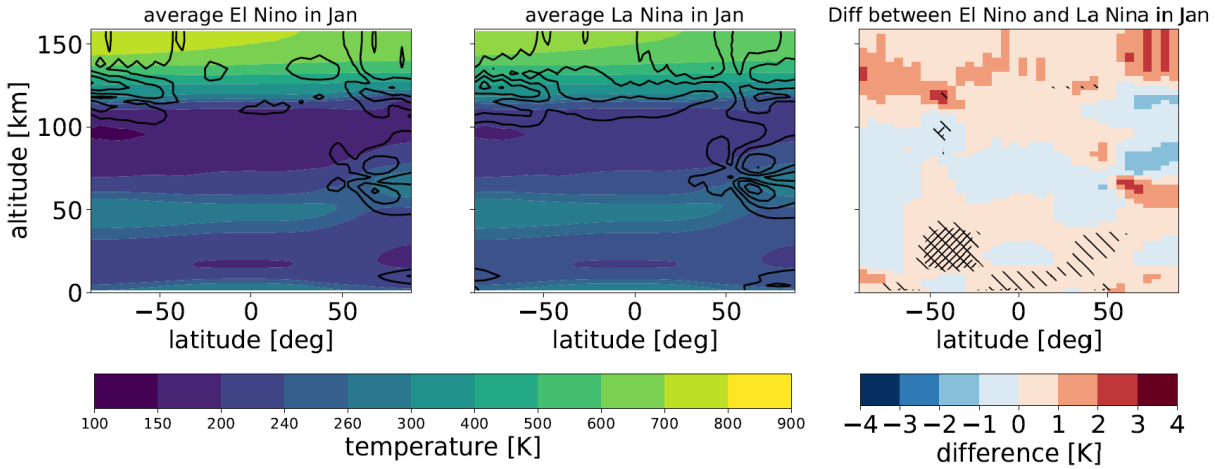

Figure 4: Average El Niño (La Niña) background temperature field without latent heat on the left (in the center), temperature difference between El Niño minus La Niña (right), Altitude in km depending on latitude in degree, temperature in K (colored), from Stober [2020]

Figure 4 shows the zonal mean background temperature field without latent heat for January. The data for the plot is averaged from five years with El Niño (1983, 1992, 1998, 2003, 2010) and five years with La Niña (1989, 1999, 2000, 2008, 2011) conditions respectively. These are used for the calculations of the latent heat comparison in chapter 4. In all calculations, only January was considered. There is a difference plot on the right site in figure 4, because the differences are hard to see in the two left plots. There is a red area around the equator directly above the surface in the difference plot. That means the temperature is higher at this site in El Niño conditions. The theory from above coincides with this result.

3 Middle and Upper Atmosphere Model MUAM

MUAM is a 3D-mechanistic nonlinear grid point model. It has a latitde resolution of 5° and a longitude resolution of 5.625°. There are 48-60 altitude levels in MUAM. For the comparison 56 altitude levels are used. MUAM has a vertical resolution of Δz =2.842 km in logarithmic pressure coordinates regardless of the choice of altitude levels.

$$z = -\mathrm{H} \cdot \ln \frac{p}{\mathrm{p_0}} \tag{1}$$

Where $\mathrm{p_0}$ is the ground reference pressure of 1000 hPa, p is the pressure and H is the scale height of 7 km.
The physics of MUAM is based on the primitive equations for a sphere with a fixed radius. The horizontal wind is calculated by the Navier–Stokes equations, the vertical wind by the continuity equation, the geopotential by the hydrostatic equation and the temperature by the first law of thermodynamics. The Matsuno-Integration scheme is used for time integration. This scheme works like a forward Euler method combined with a backward Euler method. For stability reasons the Courant–Friedrichs–Lewy condition is checked every time step. Gravity waves are parameterized according to Lindzen [1981] for stratosphere and mesosphere and according to Yiğit *et al.* [2008] for thermosphere.

The temperature under 10 km height is nudged for a more realistic troposphere. The reanalysis data for the nudging is provided by ERA (state-of-the-art reanalysis product). Modern-Era Retrospective Analysis for Research and Applications (MERRA) calculates latent heating rates by the following empirical formula:

$$J(z, \lambda, \phi) = J_z(z) \cdot J_{\lambda\phi}(\lambda, \phi) \tag{2}$$

with:

$$J_z(z) = \mathrm{A} \cdot \left(\exp\Big[-\Big(\frac{z - 6.5}{5.39} \Big)^2 \Big] - 0.23 \cdot \exp\Big(-\frac{z}{1.31} \Big) \right) \tag{3}$$

$J_{\lambda\phi}(\lambda, \phi)$ is the observed longitude/latitude distribution of the precipitation rate near the ground. $J_z(z)$ is the vertical distribution of latent heating rates depending on the precipitation rate z.

4 Comparison with and without latent heat

Five years with El Niño and five years with La Niña conditions were used. The mean values are the averaged values for the five years. The same El Niño and La Niña years like in figure 4 were used.

4.1 Amplitude

4.1.1 Temperature

The Amplitude of an atmospheric tide is the deviation from the actual value of the parameter to the mean value. The amplitude of the temperature for DT in figure 5 with latent heat during El Niño starts being detectable from the scale bar above approximately 20 km in the area of the equator. From this height the amplitude reaches 0.5 K. At around 45 to 50 km height the amplitude of the temperatur reaches in any latitude at least 0.5 K, except for the poles. Below 120 km the maximum amplitude is less than 15 K. Above this height amplitude values of more than 30 K are calculated. The amplitude increases with increasing height. That result coinsides well with the theory from above. There are approximately the same amplitude distributions and properties in figure 5 during El Niño without latent heat detectable. The changes are more obvious in the difference plot. There is almost no difference up to 100 km height. The highest differences occur in more than 120 km where the highest amplitudes occur too. There are more and stronger positive differences in this area. The maximum difference is 1.2 K, but the maximum amplitude is more than 30 K in this region. So there is a small positiv change due to latent heat. As expected, latent heat forces larger amplitudes. Figure 5 at the bottom shows the amplitude of the temperature for DT during La Niña. There are approximately the same DT calculated with and without latent heat for both El Niño and La Niña. The amplitude also increases with increasing height. The highest differences again concentrate on the area with the highest amplitudes in more than 120 km height. The maximum difference is 1.2 K with amplitudes greater than 30 K for this region. These are the same values as for El Niño.

Figure 6 shows the amplitude of the temperature for SDT. The scale bar of the temperature of the amplitude is the same for comparability. How assumed, the area of large amplitudes is smaller for SDT than for DT. During El Niño conditions amplitudes with values higher than 0.5 K can be seen above 40 km height. The largest amplitudes are above 120 km height. Above 140 km height and between 0° and 50° north latitude the values of the amplitudes are partly higher than 30 K for both with and without latent heating. The differences are maily positive with maximum values of 0.9 K. The areas of the highest differences and largest amplitudes are not the same, but close together. There are still amplitudes of more than 15 K in the area of the highest differences. Furthermore there are more negative differences for SDT than for DT. On the whole the positive dif-

ferences prevail. So there are again larger amplitudes due to latent heat. During La Niña the amplitudes of the temperature for SDT with and without latent heat are similar to El Niño conditions, except for two things. First, the maximum difference between with and without latent heat is about 0.1 K higher than for El Niño. Second, there are maximum values for the amplitude with more than 30 K below 140 km between 0° and 20° south latitude.

Figure 7 shows the amplitude of the temperature for TDT. During El Niño conditions amplitudes with values higher than 0.5 K can be seen above approximately 90 km height. Maximum amplitudes of 15 K to 20 K are reached in around 150 km height between 10° and 40° south latitude for both with and without latent heat. There are other areas with large amplitudes of maximum 10 K to 15 K above 120 km. No amplitudes larger than 20 K are calculated. The highest differences concentrate on the areas with the largest amplitudes. The maximum difference for EL Niño conditions is 1.2 K. During La Niña conditions maximum amplitudes of around 20 K to 25 K are reached in approximately 160 km height and 20° south latitude. The maximum difference is 1.3 K. There are no significant negative differences for both conditions.

Figure 8 shows the amplitude of the temperature for QDT. The amplitudes during both conditions El Niño and La Niña are smaller than TDT, SDT, and DT. Amplitude values of at least 0.5 K occur from an altitude of 100 km. Maximum values of 5 K to 10 K for the amplitude are reached above 130 km. The highest differences are located in the same areas where the largest amplitudes occur in above 120 km height. The highest differences are positive with a maximum difference of 1 K for both El Niño and La Niña.

Hagan & Forbes [2002] and Hagan & Forbes [2003] found amplitude variations of the temperature of 5 K to 15 K for DT and SDT due to latent heat. In this elaboration the maximum difference is 1.2 K for DT and 1.0 K for SDT. Smaller differences were to be expected in MUAM. Hagan & Forbes [2002] and Hagan & Forbes [2003] used five additional nonmigrating diurnal components. The forcing by these additional components led to larger amplitudes.
Considering El Niño and La Niña conditions provides a greater amount of information about tides since these conditions are one of strongest natural climate fluctuations with global impacts. However, the same formula (formula 2) was used for latent heating during El Niño and La Niña conditions. This formula has a spatial dependence, but it is not time dependent. Therefore the differences between both conditions should be small, which they are. In the following sections just El Niño conditions are considered.

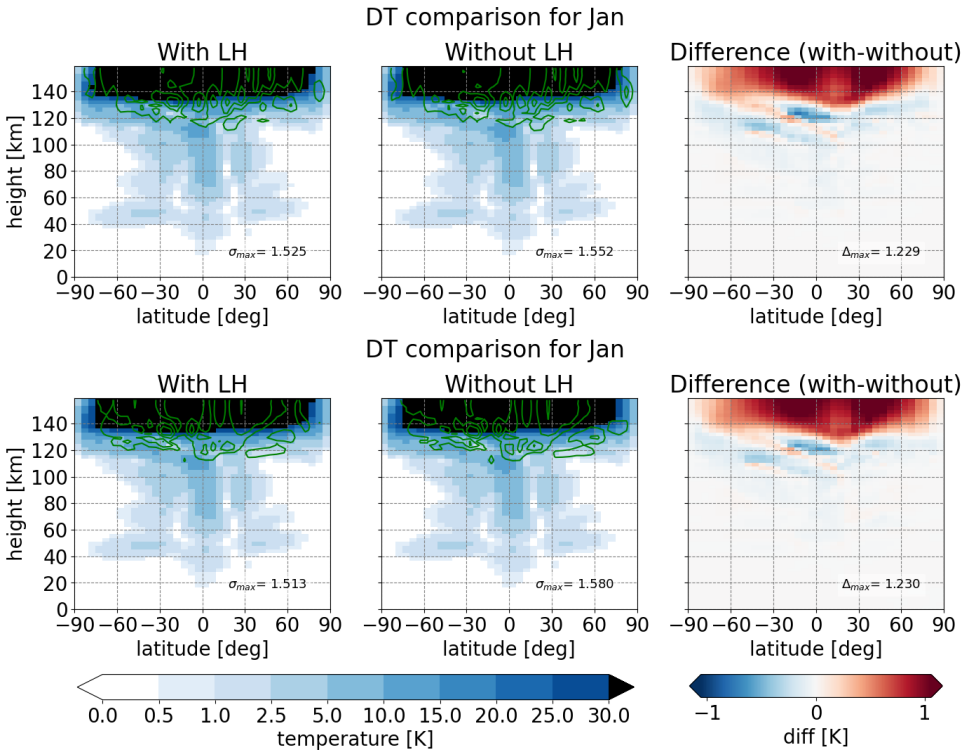

Figure 5: Zonal mean values of the amplitude of the Temperature in K for DT during El Niño (above) and La Niña (below) with latent heat (left), without latent heat (center) and the difference with minus without latent heat (right), depending on height in km and latitude in degree, green lines are standard deviations, maximum standard deviation $\sigma_{\max}$ and maximum difference $\Delta_{\max}$ are printed in the plot

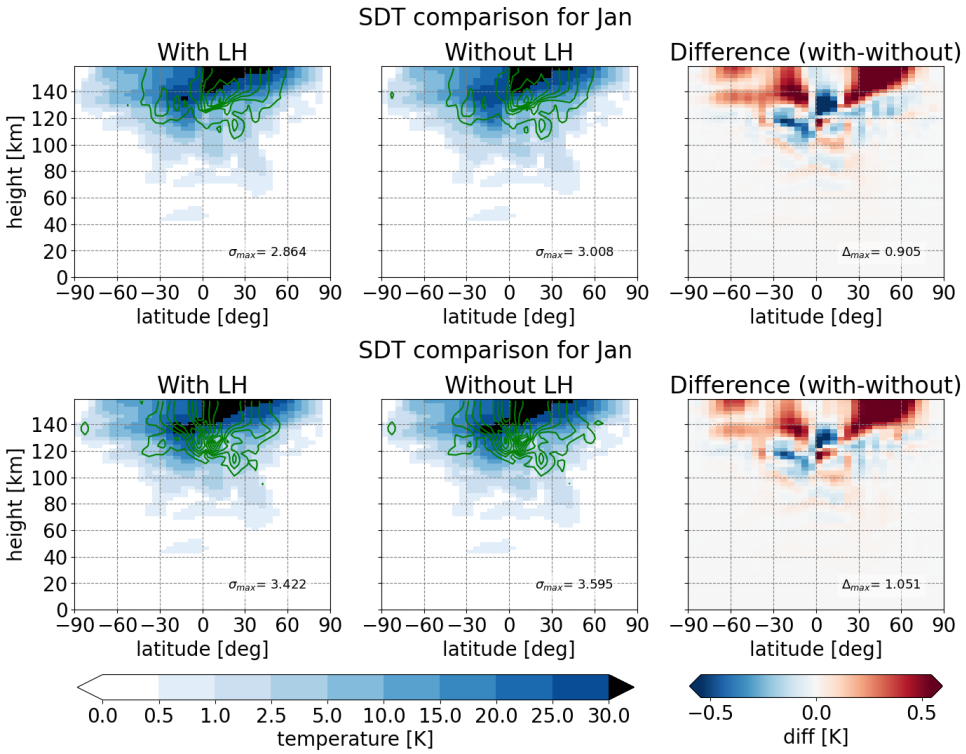

Figure 6: Like figure 5 but for SDT

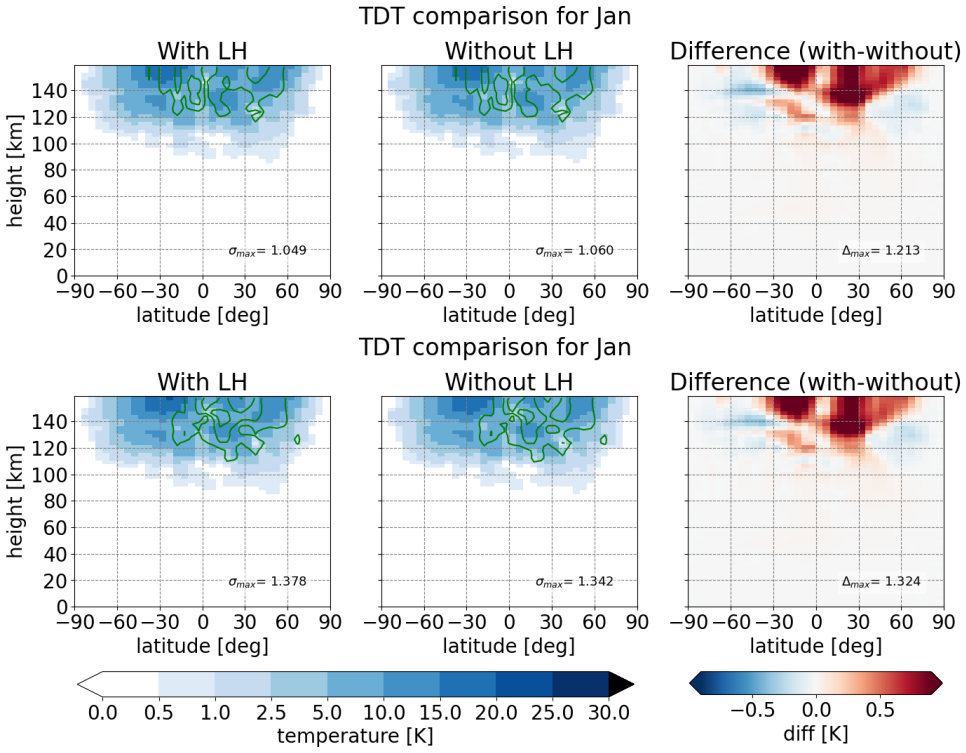

Figure 7: Like figure 5 but for TDT

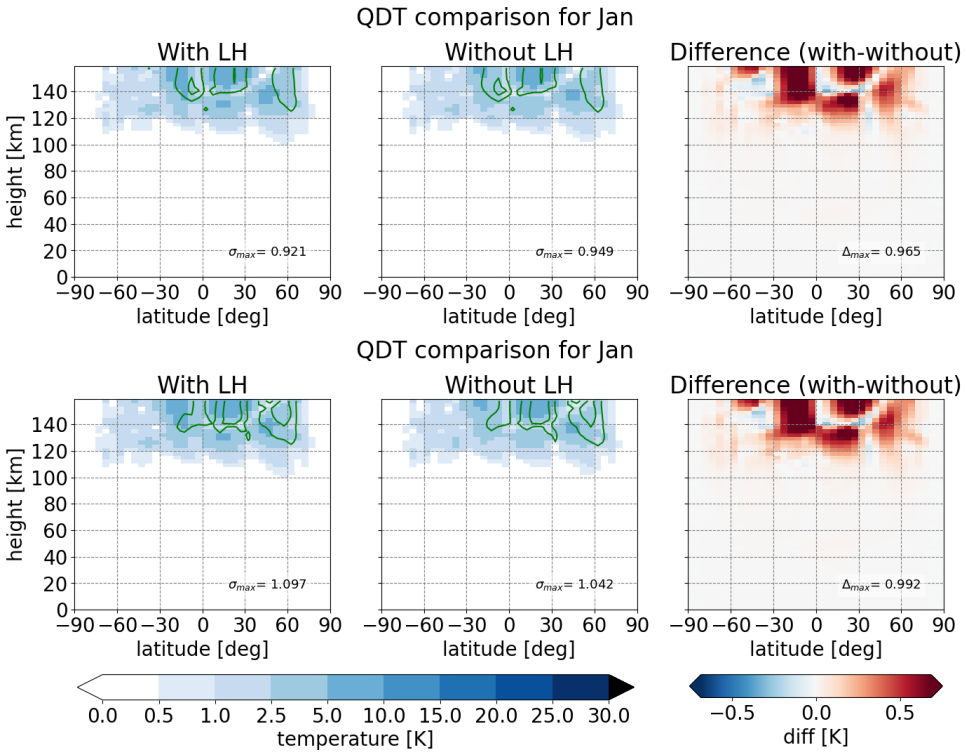

Figure 8: Like figure 5 but for QDT

4.1.2 Wind

Figure 9 shows the amplitude of the zonal wind for DT. There is a similar distribution of amplitutes with and without latent heat. Above 40 km height the zonal wind exceeds 3 $\mathrm{m\,s^{-1}}$ in several latitudes. The zonal wind only exceeds 3 $\mathrm{m\,s^{-1}}$ above 60 km on the equator and above 100 km near to the north pole. Maximum values of the zonal wind of more than 36 $\mathrm{m\,s^{-1}}$ are located above 130 km near the poles and from 140 km height in all latitudes. The difference plot on the right shows similar results like for the temperature. The highest differences are located in areas with the largest amplitudes. Around 140 km height and 30° north latitude there is a strong negative difference. Nevertheless, the differences are mostly positive, which means a larger amplitute with latent heat. The maximum difference is 1.8 $\mathrm{m\,s^{-1}}$.

Figure 10 shows the amplitude of the zonal wind for SDT. Above 60 km height the zonal wind exceeds 3 $\mathrm{m\,s^{-1}}$ at 60° north latitude. This minimum detectable amplitude value starts on the poles in more than approximately 140 km height. There are two areas with maximum values of more than 36 $\mathrm{m\,s^{-1}}$. One is located at around 120 km height between 15° and 40° south latitude. The other one is larger and starts from 150 km height between 35° south and 70° north latitude for both with and without latent heat. The area of maximum values for amplitude is smaller compared to DT. In the larger area there is mainly a positive difference to record. In the smaller area there is a slighty negative difference. The maximum difference is 1.8 $\mathrm{m\,s^{-1}}$.

Figure 11 shows the amplitude of the zonal wind for TDT. In this plot the decrease of the amplitude with decreasing period is easy to see. Minimum amplitudes detectable by the scale bar start at 90 km to 100 km height. Maximum values of 15 $\mathrm{m\,s^{-1}}$ to 18 $\mathrm{m\,s^{-1}}$ are represented for the amplitude in several areas. At around 140 km height and 30° north latitude there is a maximum amplitude of 15 $\mathrm{m\,s^{-1}}$ to 18 $\mathrm{m\,s^{-1}}$ in the plot with latent heat and 12 $\mathrm{m\,s^{-1}}$ to 15 $\mathrm{m\,s^{-1}}$ in the plot without latent heat. Indeed, there are positive differences in this area in the right plot, and there are more areas with positive differences. From 120 km height at around 50° south latitude there are negative differences. On the whole, the positive differences dominate. The maximum difference is 1.6 $\mathrm{m\,s^{-1}}$.

Figure 12 shows the amplitude of the zonal wind for QDT. Amplitudes are hardly to see with and without latent heat, because they are too small. The maximum values for the amplitudes are 9 $\mathrm{m\,s^{-1}}$ to 12 $\mathrm{m\,s^{-1}}$. However, the differences are not smaller than for DT, SDT or TDT. The maximum difference is 1.8 $\mathrm{m\,s^{-1}}$. The differences are almost exclusively positive.

Figure 13 shows the amplitude of the meridional wind for DT. The distributions of the amplitudes with and without latent heat are similar. There is almost no meridional amplitude in any height on the equator. The minimum amplitude of 3 $\mathrm{m\,s^{-1}}$ is reached from approximately 40 km height. There are four areas of higher values for the amplitudes which are quite axially symmetrical to the equator. Two areas are located between 60 km and 120 km height at approximately 15° south and north latitude with maximum amplitudes of 30 $\mathrm{m\,s^{-1}}$ to 33 $\mathrm{m\,s^{-1}}$. The other two areas are located in more than 130 km height between 15° and 90° south and north latitude with maximum amplitudes of more than 36 $\mathrm{m\,s^{-1}}$. This applies to both with and without latent heat. There are positive differences in the last two areas with the higher amplitudes. Beside these two, differences occur with changing signs. Positive differences dominate in areas with the largest amplitudes. The maximum difference is 1.6 $\mathrm{m\,s^{-1}}$.

Figure 14 shows the amplitude of the meridional wind for SDT. The minimum amplitude of 3 $\mathrm{m\,s^{-1}}$ is reached from approximately 60 km height. This is 20 km higher than for DT. There are three areas with amplitudes larger than 36 $\mathrm{m\,s^{-1}}$. One is located at 120 km height at 30° south latitude. In this area the differences between with and without latent heat are negative. The other two areas are higher than 140 km at 30° south latitude and 60° north latitude. These two areas have larger absolute values of the difference compared to the first area with negative differences. The maximum difference is 1.0 $\mathrm{m\,s^{-1}}$.

Figure 15 and figure 16 show the amplitudes of the meridional wind for TDT and QDT. Amplitudes with values higher than 3 $\mathrm{m\,s^{-1}}$ can be seen above approximately 100 km height for TDT and above 120 km height for QDT for both with and without latent heat.

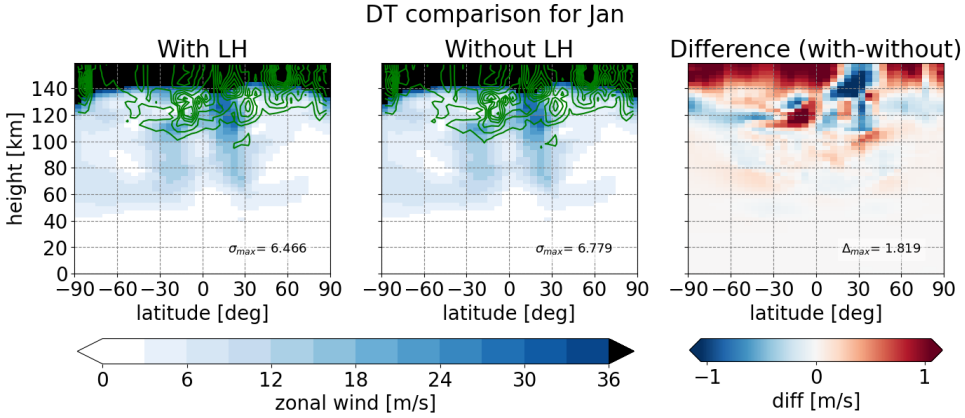

Figure 9: Zonal mean values of the amplitude of the zonal wind in $\mathrm{m\,s^{-1}}$ for DT during El Niño with latent heat (left), without latent heat (center) and the difference with minus without latent heat (right), depending on height in km and latitude in degree, green lines are standard deviations, maximum standard deviation $\sigma_{\max}$ and maximum difference $\Delta_{\max}$ are printed in the plot

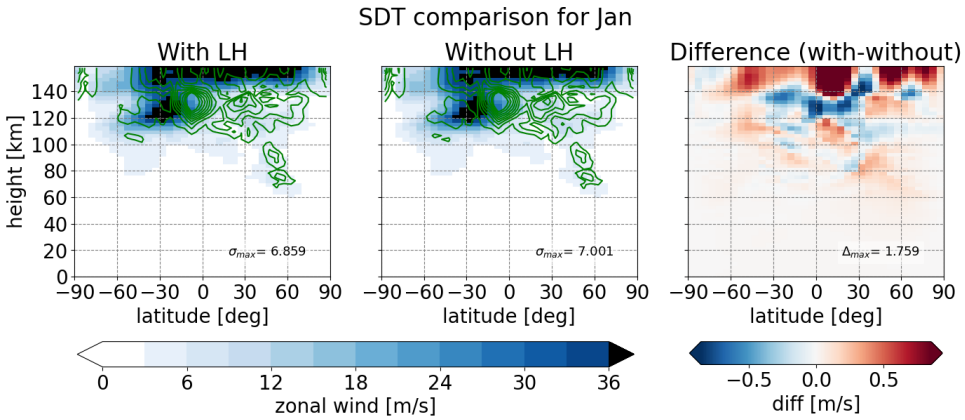

Figure 10: Like figure 9 but for SDT

The maximum value of the amplitude is 12 $\mathrm{m\,s^{-1}}$ to 15 $\mathrm{m\,s^{-1}}$ for TDT and 6 $\mathrm{m\,s^{-1}}$ to 9 $\mathrm{m\,s^{-1}}$ for QDT. A decrease of the amplitude compared to SDT and DT can be observed. The differences between with and without latent heat are mainly located in areas with largest amplitudes. The positive differences are superior to the negative ones. The maximum differences are 1.5 $\mathrm{m\,s^{-1}}$ for TDT and 1.2 $\mathrm{m\,s^{-1}}$ for QDT.

Hagan & Forbes [2002] and Hagan & Forbes [2003] found amplitude variations of the wind of 10 $\mathrm{m\,s^{-1}}$ to 20 $\mathrm{m\,s^{-1}}$ for DT and SDT due to latent heat. In this elaboration the maximum difference is 1.8 $\mathrm{m\,s^{-1}}$ for zonal wind and 1.6 $\mathrm{m\,s^{-1}}$ for meridional wind. The differences, calculated by MUAM, are smaller. One reason again are the five additional nonmigrating diurnal components used by Hagan & Forbes [2002] and Hagan & Forbes [2003]. Furthermore, MUAM is not designed to calculate large differences by just adding one component for latent heating.

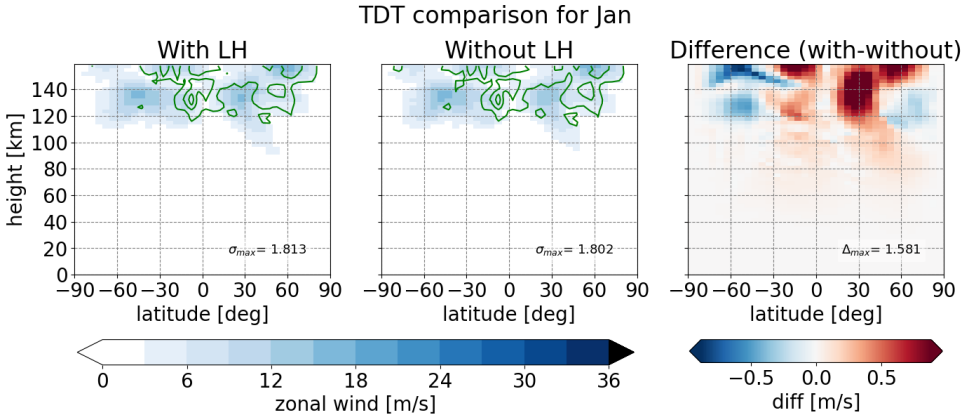

Figure 11: Like figure 9 but for TDT

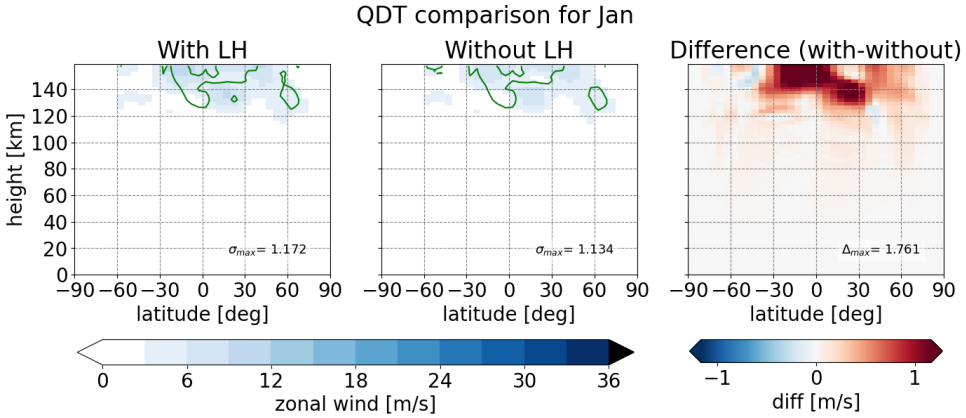

Figure 12: Like figure 9 but for QDT

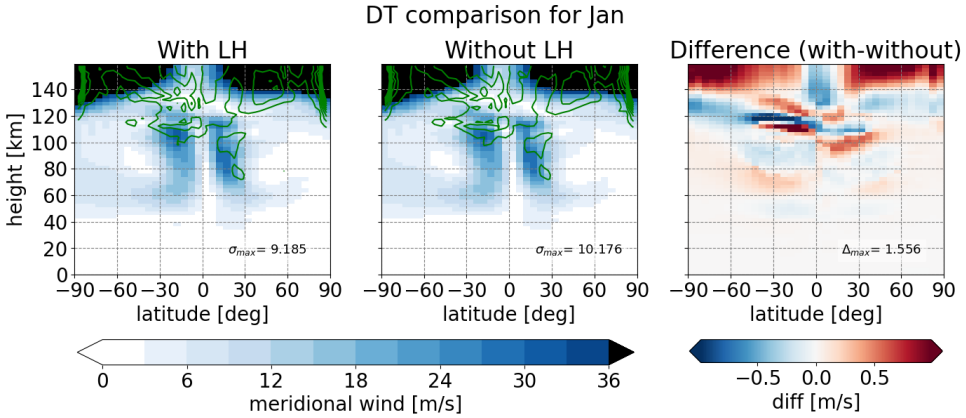

Figure 13: Zonal mean values of the amplitude of the meridional wind in $\mathrm{m\,s^{-1}}$ for DT during El Niño with latent heat (left), without latent heat (center) and the difference with minus without latent heat (right), depending on height in km and latitude in degree, green lines are standard deviations, maximum standard deviation $\sigma_{\max}$ and maximum difference $\Delta_{\max}$ are printed in the plot

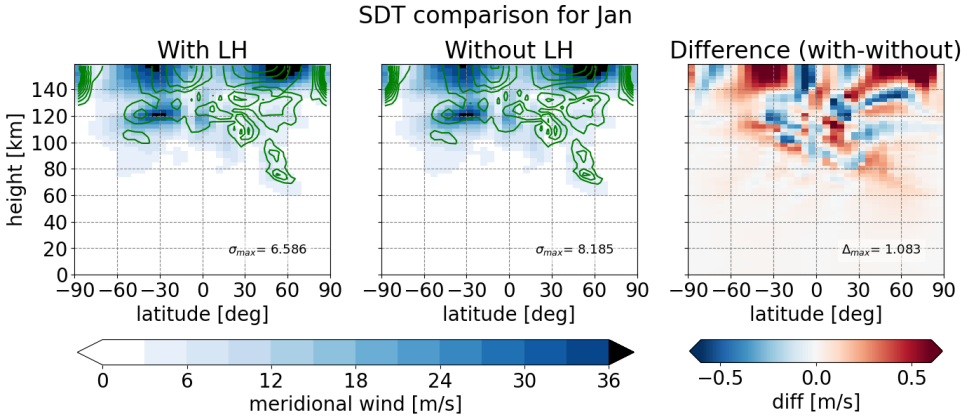

Figure 14: Like figure 13 but for SDT

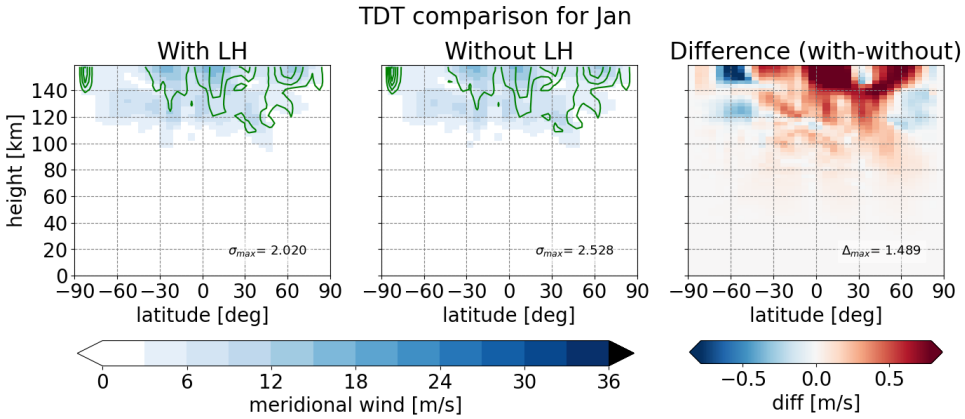

Figure 15: Like figure 13 but for TDT

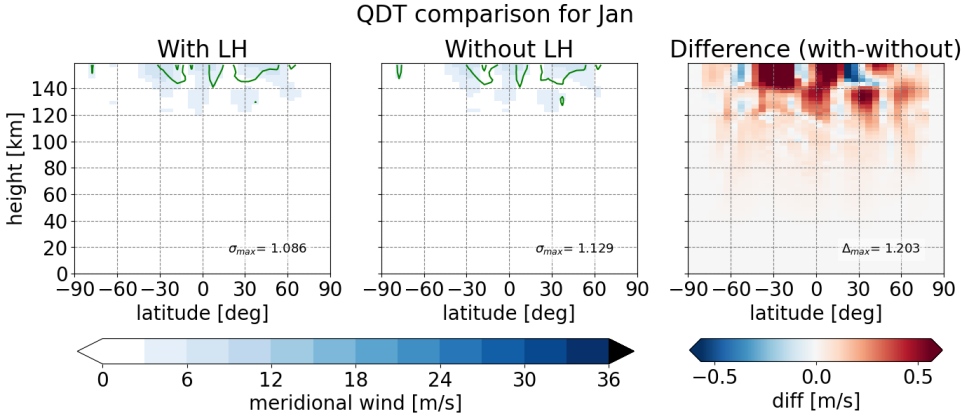

Figure 16: Like figure 13 but for QDT

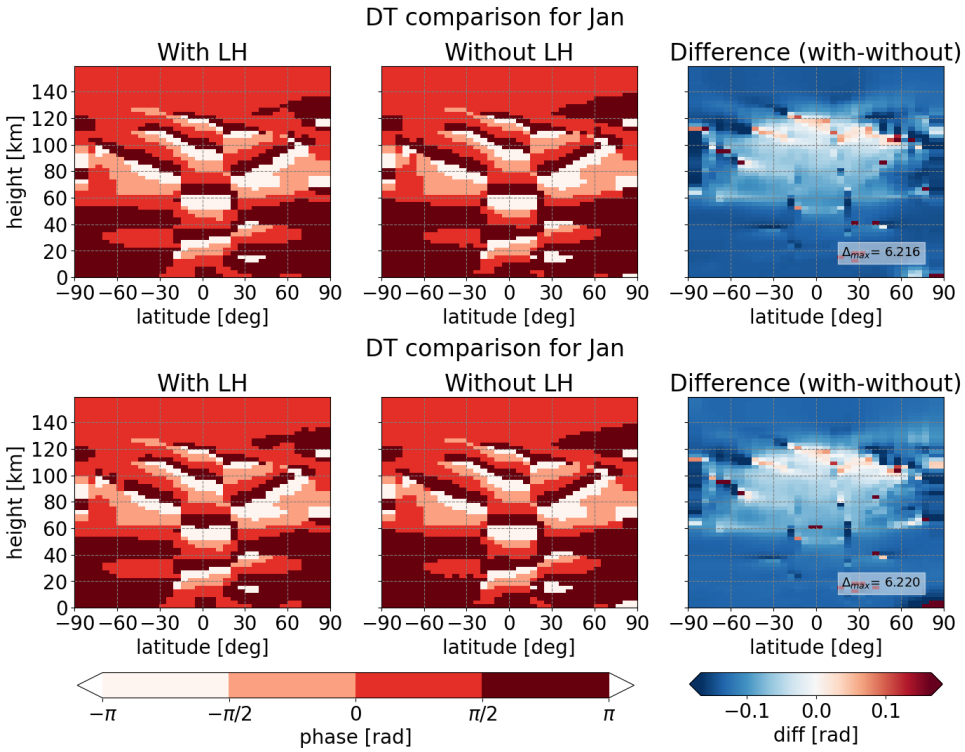

Figure 17: Zonal mean values of the phase of the Temperature in radian for DT during El Niño (above) and La Niña (below) with latent heat (left), without latent heat (center) and the difference with minus without latent heat (right), depending on height in km and latitude in degree, maximum difference $\Delta_{\max}$ is printed in the right plot

4.2 Phase

Figure 17 shows the phase of the temperature and the difference of the phase with and without latent heat for DT during El Niño and La Niña. The phases calculated with and without latent heat look similar. There are no huge phase shifts and no significant differences between El Niño and La Niña conditions. The difference plot on the right side confirms it. There are differences of -0.1 radian, which is approximately $\frac{\pi}{32}$. However, the maximum difference is 6.2 radian. This is approximately 2π. But this is due to calculation errors when forming the difference. There is a jump from π to $-\pi$.
These errors are clearly visible in figure 18, where the range of the scale bar has changed. In this figure the bluish background is almost invisible. As expected, the phase does not change dramatically. An additional component forces higher amplitudes, but does not change the phase at all. It remains the same wave.

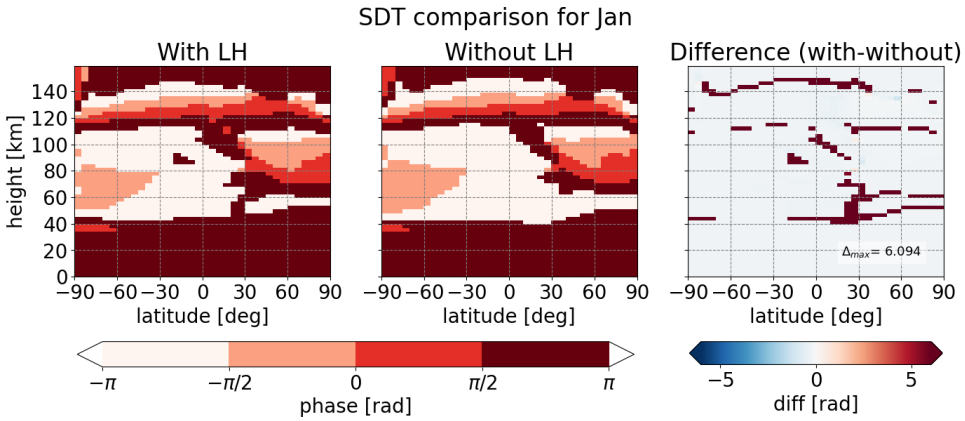

Figure 18: Zonal mean values of the phase of the zonal wind in radian for SDT during El Niño with latent heat (left), without latent heat (center) and the difference with minus without latent heat (right), depending on height in km and latitude in degree, maximum difference $\Delta_{\max}$ is printed in the right plot

5 Conclusions

Data of five years with El Niño and La Niña conditions were used to calculate the impact of latent heat on tides in MUAM. Simulations with and without latent-heating parameterization with MUAM were made.

There is an effect of latent heat on tides. According to Hagan & Forbes [2002], the variations are most apparent at a height of 80 km to 150 km. That result can be confirmed with this elaboration using MUAM. However, the variations of the amplitudes are smaller with the parameterization described in section 3 compared to Hagan & Forbes [2002].
The following three conclusions can be made. First, the amplitudes decrease with a decreasing period of the tide. Second, latent heat increases the values of the amplitudes of the tides overall. This is only a small effect, but it has an impact on the tides. The difference of the simulation results with and without latent-heating parameterization does not decrease with decreasing period of the tide. So the biggest differences alternate between DT, SDT, TDT and QDT. Third, there are negligible phase changes. The tides remain, but with slightly larger amplitudes.
There has to be more investigation of the exact interactions of the troposphere with the middle and upper atmosphere to confirm the quantitative impact of latent heat on atmospheric tides. Periods longer than 5 or 10 years and a time-dependent formula for the latent-heating parameterization could result in increased accuracy.

References

Ammann, Christoph. 2021. *Was ist El Niño?* Abrufbar unter: `http://www.elnino.info/k1.php`.

Andrews, David G, Holton, James R, & Leovy, Conway B. 1987. *Middle atmosphere dynamics*. Academic press.

Ermakova, Tatiana S, Aniskina, Olga G, Statnaia, Irina A, Motsakov, Maxim A, & Pogoreltsev, Alexander I. 2019. Simulation of the ENSO influence on the extra-tropical middle atmosphere. *Earth, Planets and Space*, **71**(1), 1–9.

Forbes, Jeffery M, Hagan, ME, Zhang, X, & Hamilton, K. 1997. Upper atmosphere tidal oscillations due to latent heat release in the tropical troposphere. *Pages 1165–1175 of: Annales Geophysicae*, vol. 15. Springer.

Forbes, Jeffrey M, *et al.* 1995. Tidal and planetary waves. *The Upper Mesosphere and Lower Thermosphere: A Review of Experiment and Theory, Geophys. Monogr. Ser*, **87**, 67–87.

Forbes, JM, Russell, J, Miyahara, S, Zhang, X, Palo, S, Mlynczak, M, Mertens, CJ, & Hagan, ME. 2006. Troposphere-thermosphere tidal coupling as measured by the SABER instrument on TIMED during July–September 2002. *Journal of Geophysical Research: Space Physics*, **111**(A10).

Gurubaran, S. Understanding Atmospheric Tides: Challenges to Middle Atmospheric Dynamicists.

Hagan, ME, & Forbes, Jeffery M. 2003. Migrating and nonmigrating semidiurnal tides in the upper atmosphere excited by tropospheric latent heat release. *Journal of Geophysical Research: Space Physics*, **108**(A2).

Hagan, ME, & Forbes, JM. 2002. Migrating and nonmigrating diurnal tides in the middle and upper atmosphere excited by tropospheric latent heat release. *Journal of Geophysical Research: Atmospheres*, **107**(D24), ACL–6.

Hamilton, Kevin. 1981. Latent heat release as a possible forcing mechanism for atmospheric tides. *Monthly Weather Review*, **109**(1), 3–17.

Latif, Mojib. 2006. Das El Niño/Southern Oscillation-Phänomen/The El Niño/Southern Oscillation Phenomenon. *Promet-Meteorologische Fortbildung*, **32**(3/4), 123–129.

Lilienthal, F. 2019. *Analysis of the Forcing Mechanisms of the Terdiurnal Solar Tide in the Middle Atmosphere*. Leipzig University.

Lindzen, Richard S. 1981. Turbulence and stress owing to gravity wave and tidal breakdown. *Journal of Geophysical Research: Oceans*, **86**(C10), 9707–9714.

Stober, Melanie. 2020. Einfluss von El Niño-Southern Oscillation auf die mittlere Atmosphäre. *Bachelor Thesis*.

Stull, Roland B, *et al.* 2018. Practical meteorology: an algebra-based survey of atmospheric science.

Tsuda, Toshitaka, & Kato, Susumu. 1989. Diurnal non-migrating tides excited by a differential heating due to land-sea distribution. *Journal of the Meteorological Society of Japan. Ser. II*, **67**(1), 43–55.

Williams, Christopher R, & Avery, Susan K. 1996. Diurnal nonmigrating tidal oscillations forced by deep convective clouds. *Journal of Geophysical Research: Atmospheres*, **101**(D2), 4079–4091.

Yiğit, Erdal, Aylward, Alan D, & Medvedev, Alexander S. 2008. Parameterization of the effects of vertically propagating gravity waves for thermosphere general circulation models: Sensitivity study. *Journal of Geophysical Research: Atmospheres*, **113**(D19).

Zhang, Xiaoli, Forbes, Jeffrey M, Hagan, Maura E, Russell III, James M, Palo, Scott E, Mertens, Christopher J, & Mlynczak, Martin G. 2006. Monthly tidal temperatures 20–120 km from TIMED/SABER. *Journal of Geophysical Research: Space Physics*, **111**(A10).

List of abbreviations

DT	Diurnal tide
ENSO	El Niño-Southern Oscillation
MERRA	Modern-Era Retrospective Analysis for Research and Applications
MUAM	Middle and Upper Atmosphere Model
QDT	Quarterdiurnal tide
SDT	Semidiurnal tide
TDT	Terdiurnal tide

List of Figures